

Melt Fracture Revisited

J. M. Greenberg^{#,*}

Department of Mathematical Sciences
Carnegie Mellon University
Pittsburgh, PA 15213

Abstract

In a previous paper the author and Demay advanced a model to explain the melt fracture instability observed when molten linear polymer melts are extruded in a capillary rheometer operating under the controlled condition that the inlet flow rate was held constant. The model postulated that the melts were a slightly compressible viscous fluid and allowed for slipping of the melt at the wall. The novel feature of that model was the use of an empirical switch law which governed the amount of wall slip. The model successfully accounted for the oscillatory behavior of the exit flow rate, typically referred to as the melt fracture instability, but did not simultaneously yield the fine scale spatial oscillations in the melt typically referred to as shark skin.

In this note a new model is advanced which simultaneously explains the melt fracture instability and shark skin phenomena. The model postulates that the polymer is a slightly compressible linearly viscous fluid but assumes no slip boundary conditions at the capillary wall. In simple shear the shear stress τ and strain rate d are assumed to be related by $d = F\tau$ where F ranges between F_2 and $F_1 > F_2$. A strain rate dependent yield function is introduced and this function governs whether F evolves towards F_2 or F_1 . This model accounts for the empirical observation that at high shears polymers align and slide more easily than at low shears and explains both the melt fracture and shark skin phenomena.

[#]This paper is dedicated to Fred Howes, my program officer at the U.S. Department of Energy, who was always supportive of my research program and whose death is sadly mourned.

^{*}This research was partially supported by the Applied Mathematical Sciences Program, U.S. Department of Energy; the Mathematics and Computer Science Division, Army Research Office; and International Programs, U.S. National Science Foundation. During the summer of 1996, the author also received generous support from CNRS to pursue this project.

DISCLAIMER

This report was prepared as an account of work sponsored by an agency of the United States Government. Neither the United States Government nor any agency thereof, nor any of their employees, makes any warranty, express or implied, or assumes any legal liability or responsibility for the accuracy, completeness, or usefulness of any information, apparatus, product, or process disclosed, or represents that its use would not infringe privately owned rights. Reference herein to any specific commercial product, process, or service by trade name, trademark, manufacturer, or otherwise does not necessarily constitute or imply its endorsement, recommendation, or favoring by the United States Government or any agency thereof. The views and opinions of authors expressed herein do not necessarily state or reflect those of the United States Government or any agency thereof.

DISCLAIMER

**Portions of this document may be illegible
in electronic image products. Images are
produced from the best available original
document.**

1 Introduction

In a previous paper [1] Greenberg and Demay advanced a model to explain the melt fracture instability observed when molten linear polymer melts are extruded in a capillary rheometer operating under the controlled condition that the inlet flow rate was held constant. Their model postulated that the melts were a slightly compressible viscous fluid and allowed for slipping of the melt at the wall. The novel feature of their model was the use of an empirical switch law which governed the amount of wall slip. Their model successfully accounted for the oscillatory behavior of the exit flow rate typically referred to as the melt fracture instability but did not simultaneously yield the fine scale spatial oscillations in the melt typically referred to as shark skin. A similar model was developed at approximately the same time by Hatzikiriakos and Dealy [2,3].

In this note, we return to the problem studied in [1] and advance a new model which simultaneously explains the melt fracture instability and shark skin phenomena. The proposed model also assumes the polymer is a slightly compressible linearly viscous fluid but assumes no slip boundary conditions at the capillary wall. We assume that in simple shear the shear stress τ and strain rate d are related by

$$\tau = \mu d \quad (1.1)$$

where

$$\mu = \frac{\mu_1 \mu_2}{\mu_1(1 - \phi) + \mu_2 \phi} \quad (1.2)$$

and

$$\mu_2 > \mu_1 > 0. \quad (1.3)$$

ϕ is interpreted as an order parameter which ranges over the interval $[0, 1]$. When $\phi = 0$ the polymer molecules are nonaligned and the fluid is highly viscous ($\mu = \mu_2$) whereas when $\phi = 1$ the polymer molecules are aligned and the fluid is less viscous ($\mu = \mu_1 < \mu_2$).

We assume that ϕ satisfies

$$\delta(\phi_t + \mathbf{u} \cdot \nabla \phi) = \frac{1}{2} (1 + \text{sign} (|\tau|_{\max} - \tau_y)) - \phi. \quad (1.4)$$

Here \mathbf{u} is the fluid velocity, $|\tau|_{\max}$ is the maximum shear stress, and τ_y is a strain rate dependent yield stress which we shall model later. (1.4) implies that if $|\tau|_{\max} < \tau_y$, then ϕ is driven to zero, whereas if $|\tau|_{\max} > \tau_y$, then ϕ is driven to one.

If we let

$$F = \frac{1}{\mu} = (F_2 + (F_1 - F_2)\phi) \quad (1.5)$$

where

$$F_2 = \frac{1}{\mu_2} < F_1 = \frac{1}{\mu_1}, \quad (1.6)$$

then (1.4) is equivalent to

$$\delta(F_t + \mathbf{u} \cdot \nabla F) = \frac{1}{2} (F_1 + F_2 + (F_1 - F_2) \text{sign} (|\tau|_{\max} - \tau_y)) - F. \quad (1.7)$$

This model accounts for the empirical observation that at high shears polymers align and slide more easily than at low shears. Equation (1.4) represents the new twist of our model and allows us to abandon the questionable assumption that slipping occurs at the capillary wall.

A nice description of the melt fracture phenomenon may be found in Joseph and Renardy [4, pp. 375-378]. They too discuss the existence critical or yield stresses which governs whether the polymer is more or less viscous. Here we quote "we can expect a migration of low-viscosity constituents into regions of high shear. These high-shear regions may take form as wet layer of small thickness or perhaps a region deficient in high molecular weights defined by large gradients of molecular weight. The slip in such layers is apparent. There is no slip surface, rather there are large gradients across narrow layers which are perceived as slips." The model we advance predicts many of these features.

2 Model Development.

Figure 2 describes the flow geometry. Our modelling effort accounts for what happens in the capillary tube and not in the reservoir.

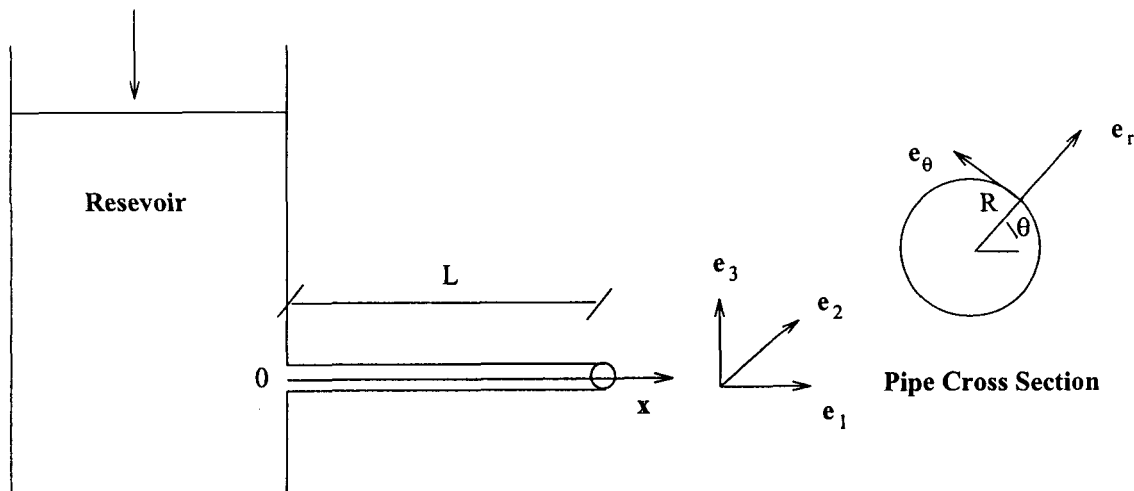


Figure 1.

We assume the flow in the capillary is axisymmetric, and that all quantities depend only on x, r and t . We let ρ denote the polymer density, p denote the pressure and assume that the velocity field \mathbf{u} and Cauchy stress tensor σ are of the form:

$$\mathbf{u} = u \mathbf{e}_1 + w \mathbf{e}_r \quad (2.1)$$

and

$$\sigma = -p(e_1 \otimes e_1 + e_r \otimes e_r + e_\theta \otimes e_\theta) + \sigma_{11}^v e_1 \otimes e_1 + \sigma_{rr}^v e_r \otimes e_r + \sigma_{\theta\theta}^v e_\theta \otimes e_\theta + \tau(e_1 \otimes e_r + e_r \otimes e_1). \quad (2.2)$$

$(\sigma_{11}^v, \sigma_{rr}^v, \sigma_{\theta\theta}^v, \tau)$ are the nonzero components of the viscous stress tensor and are related to u and w by

$$\left. \begin{aligned} \frac{2}{3} \frac{\partial u}{\partial x} - \frac{1}{3} \frac{1}{r} \frac{\partial}{\partial r}(rw) &= \frac{F}{2} \sigma_{11}^v \\ \frac{2}{3} \frac{\partial w}{\partial r} - \frac{1}{3} \frac{w}{r} - \frac{1}{3} \frac{\partial u}{\partial x} &= \frac{F}{2} \sigma_{rr}^v \\ \frac{2}{3} \frac{w}{r} - \frac{1}{3} \frac{\partial w}{\partial r} - \frac{1}{3} \frac{\partial u}{\partial x} &= \frac{F}{2} \sigma_{\theta\theta}^v \\ \frac{\partial u}{\partial r} + \frac{\partial w}{\partial x} &= F\tau \end{aligned} \right\} \quad (2.3)$$

and

where once again F satisfies (1.7). The constitutive equation (2.3) yields a trace free viscous stress tensor and thus satisfies the "Stokes" hypothesis.

The governing equations are the continuity equation

$$(C) \quad \frac{\partial \rho}{\partial t} + \frac{\partial}{\partial x}(\rho u) + \frac{1}{r} \frac{\partial}{\partial r}(r \rho w) = 0,$$

and balance of momentum in the directions e_1 and e_r . At the boundary, $r = R$, we assume that

$$(BC) \quad u(x, R, t) = 0 \text{ and } w(x, R, t) = 0.$$

¹ $e_1 = (1, 0, 0)$, $e_r = (0, \cos \theta, \sin \theta)$ and $e_\theta = (0, -\sin \theta \cos \theta)$ and for any vectors $a = (a_1, a_2, a_3)$ and $b = (b_1, b_2, b_3)$, $a \otimes b = a^T b$ where $a^T = \begin{pmatrix} a_1 \\ a_2 \\ a_3 \end{pmatrix}$.

We further assume that the polymer is slightly compressible, that is the following equation of state holds between the density and pressure:

$$(EOS) \quad \rho = \rho_0 \left(1 + \frac{2\epsilon_1 p}{p_0} \right).$$

Here, ρ_0 and p_0 are reference values of the density and pressure and $0 < \epsilon_1 \ll 1$ is a dimensionless small parameter.

To assess which terms in this system are important and which may be neglected, we cast the system in dimensionless form. We let

$$x = Lx_1, \quad r = Rr_1, \quad \text{and} \quad t = \frac{\epsilon_1}{p_0 \epsilon_2^2 F_2} t_1 \quad (2.4)$$

and

$$\rho = \rho_0 \rho_1, \quad u = p_0 R \epsilon_2 F_2 u_1, \quad w = p_0 R \epsilon_2^2 F_2 w_1, \quad p = 2p_0 p_1 \quad \text{and} \quad F = F_2 D \quad (2.5)$$

where D ranges from 1 to $D_1 = F_1/F_2 > 1$ and $0 < \epsilon_2 = \frac{R}{L} \ll 1$.²

With these scalings the shear stress becomes

$$\tau = p_0 \epsilon_2 \tau_1 \quad (2.6)$$

where

$$\left(\frac{\partial u_1}{\partial r_1} + \epsilon_2 \frac{\partial w_1}{\partial x_1} \right) = D \tau_1. \quad (2.7)$$

The remaining viscous stresses are $O(p_0 \epsilon_2^2)$ and are thus neglectable relative to the pressure and shear stress. With this scaling we may replace the maximum shear stress $|\tau|_{\max}$ in (1.7) by $p_0 \epsilon_2 |\tau_1|$.

The equation of state transforms to

$$\rho_1 = 1 + 2\epsilon_1 p_1. \quad (2.8)$$

The assumptions $0 < \epsilon_1 \ll 1$ and $0 < \epsilon_2 \ll 1$ imply that to lowest order in the ϵ 's the continuity equation is reduced to

$$\frac{2\partial p_1}{\partial t_1} + \frac{\partial u_1}{\partial x_1} + \frac{1}{r_1} \frac{\partial}{\partial r_1} (r_1 w_1) = 0. \quad (2.9)$$

If we further make the lubrication hypothesis $0 < \epsilon_2^2/\epsilon_1 \ll 1$, then balance of momentum in the direction e_r implies that

$$p_1 = p_1(x_1, t_1) \quad (2.10)$$

while balance of momentum in the direction e_1 takes the form

²The length of scale L in the “ x ” direction may be thought of as the capillary length or the length of a typical disturbance in the “ x ” direction.

$$\frac{1}{r_1} \frac{\partial}{\partial r_1} (r_1 \tau_1) = 2 \frac{\partial p_1}{\partial x_1}. \quad (2.11)$$

Equations (2.10) and (2.11) then yield

$$\tau_1 = r_1 \frac{\partial p_1}{\partial x_1} \quad (2.12)$$

and equations (2.7) and (2.12) imply, to lowest order in the ϵ 's, that

$$d_1 = \frac{\partial u_1}{\partial r_1} = D\tau_1 = Dr_1 \frac{\partial p_1}{\partial x_1}. \quad (2.13)$$

Equation (2.13), together with $(BC)_1$, implies that the velocity u_1 is given by

$$u_1(x_1, r_1, t_1) = -\frac{\partial p_1}{\partial x_1} \int_{r_1}^1 D(x_1, s, t) s ds$$

and the flow rate, q_1 , by

$$q_1(x_1, t) \stackrel{\text{def}}{=} \int_0^1 r_1 u_1(x_1, r_1, t_1) dr_1 = -\frac{1}{8} D_3(x_1, t_1) \frac{\partial p_1}{\partial x_1}(x_1, t_1) \quad (2.14)$$

where D_3 is the cross-sectional average

$$D_3(x_1, t_1) \stackrel{\text{def}}{=} 4 \int_0^1 r_1^3 D(x_1, r_1, t_1) dr_1 \quad (2.15)$$

If we multiply (2.9) by r_1 , integrate the resulting equation from $r_1 = 0$ to $r_1 = 1$, and exploit the fact that $r_1 w_1$ vanishes at $r_1 = 0$ and $r_1 = 1$, we obtain the following equation for p_1 :

$$\frac{\partial p_1}{\partial t_1} - \frac{1}{8} \frac{\partial}{\partial x_1} \left(D_3 \frac{\partial p_1}{\partial x_1} \right) = 0. \quad (2.16)$$

Under the scaling (2.4) and (2.5) equation (1.7) transforms, to lowest order in the ϵ 's, to

$$\epsilon_3 \frac{\partial D}{\partial t_1} = \frac{1}{2} (D_1 + 1 + (D_1 - 1)\text{sign}(|\tau_1| - \hat{\tau}_y)) - D. \quad (2.17)$$

Here

$$\epsilon_3 = \frac{\delta p_0 \epsilon_2^2 F_2}{\epsilon_1}, \quad (2.18)$$

τ_1 is the scaled $x - r$ shear stress, and $\hat{\tau}_y$ is the scaled yield stress defined by $\tau_y = p_0 \epsilon_2 \hat{\tau}_y$.

Moreover (2.17), when combined with (2.12), implies that D satisfies

$$\epsilon_3 \frac{\partial D}{\partial t_1}(x_1, r_1, t_1) = \frac{1}{2} \left(D_1 + 1 + (D_1 - 1)\text{sign} \left(r_1 \left| \frac{\partial p_1}{\partial x_1} \right| - \hat{\tau}_y \right) \right) - D. \quad (2.19)$$

Up to this point we have deferred a discussion of the behavior of the yield stress τ_y on the strain rate. In a simple shear experiment a plausible yield function is given by

$$\tau_y(|d|) = \begin{cases} \sigma_2, & 0 \leq |d| \leq F_2\sigma_2 \\ \sigma_2 + \left(\frac{\sigma_1 - \sigma_2}{F_1\sigma_1 - F_2\sigma_2} \right) (|d|) - F_2\sigma_2, & F_2\sigma_2 \leq |d| \leq F_1\sigma_1 \\ \sigma_1, & F_1\sigma_1 \leq |d| \end{cases}$$

where $\sigma_1 < \sigma_2$, $F_2 < F_1$, and $F_2\sigma_2 < F_1\sigma_1$, and with the scalings (2.4)-(2.6) and $\tau_y = p_0\epsilon_2\hat{\tau}_y$ this would yield the scaled yield stress

$$\hat{\tau}_y(|d_1|) = \begin{cases} s_2, & 0 \leq |d_1| < s_2 \\ s_2 + \frac{(s_1 - s_2)}{(D_1s_1 - s_2)} (|d_1| - s_2), & s_2 \leq |d_1| \leq D_1s_1 \\ s_1, & D_1s_1 \leq |d_1| \end{cases} \quad (2.20)$$

where

$$s_2 = \frac{\sigma_2}{p_0\epsilon_2} > s_1 = \frac{\sigma_1}{p_0\epsilon_2} \text{ and } D_1 = \frac{F_1}{F_2} > 1 \quad (2.21)$$

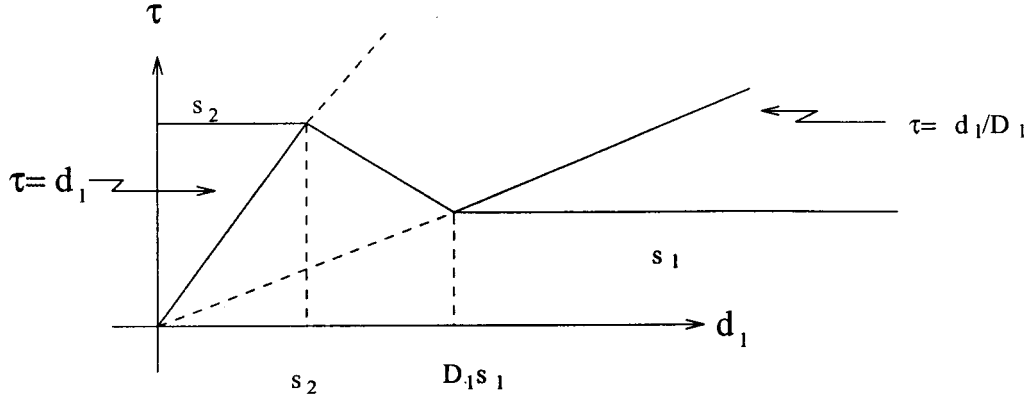


Figure 2.

One could attempt to use the scaled yield stress directly in (2.19). If one does this, then (2.13), (2.19)-(2.21) would imply the following evolution equation for D :

$$\epsilon_3 \frac{\partial D}{\partial t} = \frac{1}{2} \left(D_1 + 1 + (D_1 - 1) \operatorname{sign} \left(r_1 \left| \frac{\partial p_1}{\partial x_1} \right| - \hat{\tau}_y \left(D r_1 \left| \frac{\partial p_1}{\partial x_1} \right| \right) \right) \right) - D \quad (2.22)$$

and our combined system would be (2.15), (2.16), and (2.20)-(2.22). The fine structure equation, (2.22), for D requires initial data $D_0(x_1, r_1) = D(x_1, r_1, 0^+)$, a quantity not easily measured.

Instead of (2.22) we seek a simpler model which doesn't require such fine structure data. We accomplish this by replacing the term $\hat{\tau} \left(D r_1 \left| \frac{\partial p_1}{\partial x_1} \right| \right)$ in (2.22) by $\hat{\tau}_y \left(D_3 r_1 \left| \frac{\partial p_1}{\partial x_1} \right| \right)$ where again D_3 is the cross-sectional average

$$D_3(x_1, t_1) = 4 \int_0^1 r_1^3 D(x_1, r_1, t_1) dr_1. \quad (2.23)$$

With this replacement we are guaranteed that the function

$$r_1 \rightarrow r_1 \left| \frac{\partial p_1}{\partial x_1} \right| (x_1, t_1) - \hat{\tau}_y \left(D_3(x_1, t_1) r_1 \left| \frac{\partial p_1}{\partial x_1} \right| (x_1, t_1) \right)$$

changes sign at most once as r_1 ranges over $[0, 1]$. With this revised model (2.22) takes the form

$$\epsilon_3 \frac{\partial D}{\partial t_1} = \begin{cases} 1 - D & , \quad 0 \leq r_1 < R_1(x_1, t_1) \\ D_1 - D & , \quad R_1 < r_1 \leq 1 \end{cases} \quad (2.24)$$

where

$$R_1(x_1, t_1) = \min (1, \bar{R}(x_1, t_1)) \quad (2.25)$$

and $\bar{R}(x_1, t_1)$ is the unique solution of

$$\bar{R}(x_1, t_1) \left| \frac{\partial p_1}{\partial x_1} \right| (x_1, t_1) = \hat{\tau}_y \left(D_3(x_1, t_1) \bar{R}(x_1, t_1) \left| \frac{\partial p_1}{\partial x_1} \right| (x_1, t_1) \right). \quad (2.26)$$

Moreover, with this revised model the cross-sectional average D_3 satisfies

$$\epsilon_3 \frac{\partial D_3}{\partial t_1} = (R_1^4 + D_1(1 - R_1^4)) - D_3. \quad (2.27)$$

In fact (2.15), (2.16), and (2.25)-(2.27) represents a closed system for the switch radius R_1 , cross-sectional average D_3 , and pressure p_1 . We solve this latter system with the following initial and boundary conditions

$$p_1(x_1, 0^+) = \hat{p}(x_1) \text{ and } D_3(x_1, 0^+) = \hat{D}_3(x_1), \quad 0 \leq x_1 \leq 1 \quad (2.28)$$

where $\hat{p}(1) = 0, \hat{p}'(x_1) \leq 0$ for $0 \leq x_1 \leq 1$ and $1 \leq \hat{D}_3(x_1) \leq D_1$ for $0 \leq x_1 \leq 1$,

$$(BC)_0 \quad -\frac{D_3(0^+, t_1)}{8} \frac{\partial p_1}{\partial x_1}(0^+, t_1) = q_0 > 0$$

and

$$(BC)_1 \quad p_1(1^-, t_1) = 0$$

We note that (2.4)₃ implies that the normalizing time scale in our problem is $T_\# = \frac{\epsilon_1}{p_0 \epsilon_2^2 F_2}$ and this number though large is small relative to the travel time of a particle through the rheometer when $F = F_2$. This latter quantity is $T_* = \frac{1}{p_0 \epsilon_2^2 F_2}$ and of course $T_\# = \epsilon_1 T_*$.

There is another important time scale in our problem, namely the relaxation time δ which appears in (1.7). This time manifests itself in the dimensionless equation (2.27) in the parameter $\epsilon_3 = \frac{\delta}{T_\#}$. In the numerical simulations given in the next section we shall assume this parameter is small. This assumption, together with $T_\# = \epsilon_1 T_*$, will allow multiple spatial oscillations or wave forms over the unit capillary length.

3 Analysis of the Model of Section 2

Our interest here is in the reduced model

$$\frac{\partial p}{\partial t} - \frac{1}{8} \frac{\partial}{\partial x} \left(D_3 \frac{\partial p}{\partial x} \right) = 0, \quad 0 < x < 1 \quad (3.1)$$

and

$$\epsilon_3 \frac{\partial D_3}{\partial t} = (R^4 + D_1 (1 - R^4)) - D_3, \quad 0 < x < 1 \quad (3.2)$$

where

$$R(x, t) = \min (1, \bar{R}(x, t)), \quad (3.3)$$

\bar{R} is the unique solution of

$$\bar{R}(x, t) \left| \frac{\partial p}{\partial x} \right| (x, t) = \hat{\tau}_y \left(D_3(x, t) \bar{R}(x, t) \left| \frac{\partial p}{\partial x} \right| (x, t) \right), \quad (3.4)$$

and $\hat{\tau}_y(\cdot)$ is the normalized yield curve

$$\hat{\tau}(d) = \begin{cases} s_2, & 0 \leq d \leq s_2 \\ s_2 + \frac{(s_1 - s_2)}{(D_1 s_1 - s_2)}(d - s_2), & s_2 \leq d \leq D_1 s_1 \\ s_1, & D_1 s_1 \leq d. \end{cases} \quad (3.5)$$

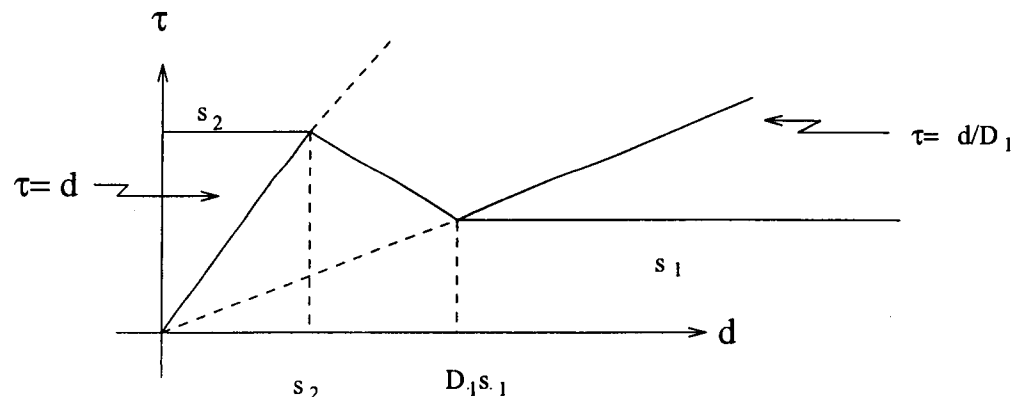


Figure 3.

Once again $s_2 > s_1$ and $1 < D_1$. This latter system is solved subject to the following initial and boundary conditions

$$p(x, 0^+) = \hat{p}(x) \text{ and } D_3(x, 0^+) = \hat{D}(x) \in [1, D_1], 0 \leq x \leq 1 \quad (3.6)$$

and

$$-\frac{1}{8}D_3(0^+, t) \frac{\partial p}{\partial x}(0^+, t) = q_0 > 0 \text{ and } p(1^-, t) = 0. \quad (3.7)$$

We assume that $\hat{p}(1) = 0$ and $\hat{p}'(x) \leq 0$, $0 \leq x \leq 1$.³

Steady Solutions

Our first task is to examine steady solutions of (3.1)-(3.5) which are compatible with (3.7). Such steady solutions are of the form

$$p = g(1 - x) \text{ and } p'(x) = -g < 0 \quad (3.8)$$

where

$$D_3 g = 8q_0, \quad D_3 = (D_1 - (D_1 - 1)R^4), \quad \text{and} \quad Rg = \hat{\tau}_y(8Rq_0). \quad (3.9)$$

Of particular interest to us here are the response curves $q_0 \rightarrow R(q_0)$ and $q_0 \rightarrow g(q_0)$.

We first note that if $0 \leq q_0 \leq \frac{s_2}{8}$, then

$$R(q_0) = 1 \text{ and } g(q_0) = 8q_0. \quad (3.10)$$

When $\frac{s_2}{8} < q_0$, (3.9) implies that R satisfies

$$\frac{8Rq_0}{(D_1 - (D_1 - 1)R^4)} = \hat{\tau}(8Rq_0) \quad (3.11)$$

and this latter equation has a unique positive solution $R = R(q_0) < 1$. Moreover, the identity

$$\begin{aligned} q_0 & \left[\frac{1}{(D_1 - (D_1 - 1)R^4(q_0))} + \frac{4(D_1 - 1)R^4(q_0)}{(D_1 - (D_1 - 1)R^4(q_0))^2} - \hat{\tau}'(8R(q_0)q_0) \right] \frac{dR}{dq_0}(q_0) \\ & = R(q_0) \left(\hat{\tau}'(8R(q_0)q_0) - \frac{1}{(D_1 - (D_1 - 1)R^4(q_0))} \right) \end{aligned}$$

³In this section we drop the subscript 1 on dimensionless quantities.

implies that $\frac{dR}{dq_0}(q_0) < 0$ on $\frac{s_2}{8} < q_0$. For suitable choices of $s_1 < s_2$ and $1 < D_1$, the curve $q_0 \rightarrow g(q_0)$ has a local maxima at $q_0 = \frac{s_2}{8}$, is monotone decreasing on $(\frac{s_2}{8}, q_*)$, and then is monotone increasing on (q_*, ∞) . Graphs of these curves when $s_1 = .75$, $s_2 = 1$, and $D_1 = 2$ are shown below.

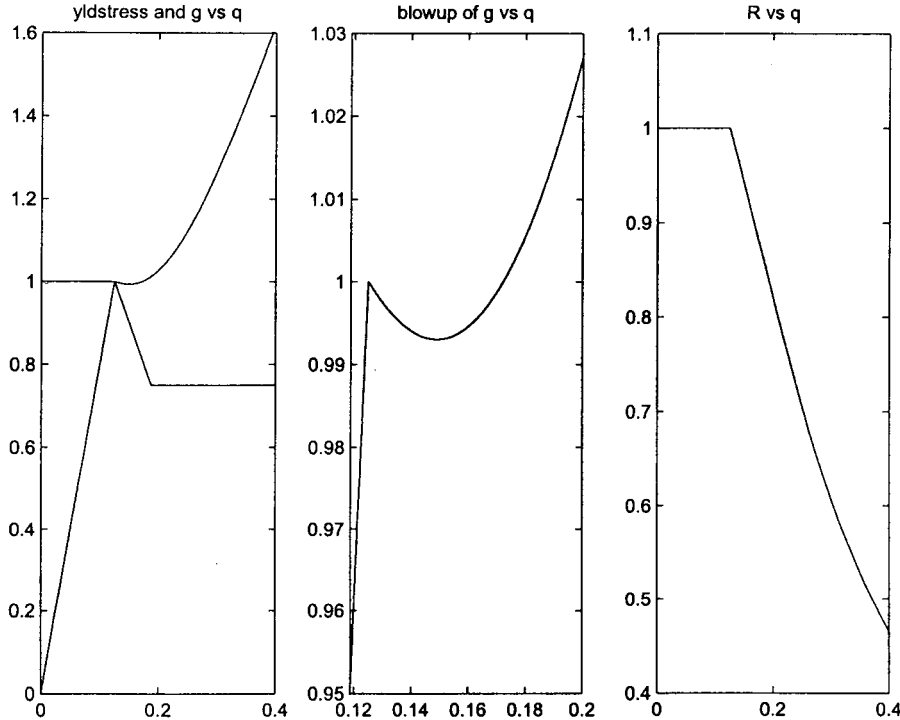


Figure 4.

It is not difficult to show that for any $q_0 > 0$ the system (3.1)-(3.7) is solvable and that the solution satisfies

$$0 \leq p(x, t) \leq p(0^+, t) \quad \text{and} \quad q(x, t) \stackrel{\text{def}}{=} -\frac{D_3}{8}(x, t) \frac{\partial p}{\partial x}(x, t) \geq 0. \quad (3.12)$$

The latter inequality follows from the observation that $q(x, t)$ satisfies

$$\left. \begin{aligned} \frac{\partial}{\partial t} \left(\frac{q}{D_3} \right) - \frac{\partial^2}{\partial x^2} q &= 0 \quad , \quad 0 < x < 1 \\ q(x, 0^+) &= -\frac{D_3(x, 0^+)}{8} \frac{\partial \hat{p}}{\partial x}(x) \geq 0 \\ q(0^+, t) &= q_0 > 0 \quad \text{and} \quad \frac{\partial q}{\partial x}(1^-, t) = 0. \end{aligned} \right\} \quad (3.13)$$

Moreover, if $q_0 \in (0, \frac{s_2}{8})$ or $q_0 \in (q_*, \infty)$, then the solution to (3.1)-(3.7) converges to the steady solution described above as time goes to infinity. Of interest to us here is what happens when the input flow rate $q_0 > 0$ lies between $\frac{s_2}{8}$ and q_* . For q_0 in this interval we get the temporal and spatial oscillations characteristic of the melt fracture instability and

shark skin phenomena. The particular character of these oscillations is dependent on the magnitude of ϵ_3 .

Computational Experiments

We use an operator splitting technique to integrate (3.1)-(3.7). If Δt is our time step, we assume that we have an approximate solution $(p^n(x), D_3^n(x), R^n(x))$, $0 \leq x \leq 1$, defined at $t_n = n\Delta t$, $n = 0, 1, 2, \dots$. During the first step we advance p keeping D_3 fixed, that is we solve

$$\frac{\partial p}{\partial t} - \frac{1}{8} \frac{\partial}{\partial x} \left(D_3 \frac{\partial p}{\partial x} \right) = 0 \quad , \quad 0 \leq t \leq \Delta t \quad (3.14)$$

subject to the boundary conditions (3.7) and the initial condition

$$p(x, 0^+) = p^n(x) \quad , \quad 0 \leq x \leq 1. \quad (3.15)$$

The updated value of the pressure, p^{n+1} , is the solution of (3.14) and (3.15) at $t = \Delta t$. During the second half step we freeze p and update D_3 , that is for each x we solve

$$\epsilon_3 \frac{\partial D_3}{\partial t}(x, t) = (D_1 - (D_1 - 1)(R^n(x))^4) - D_3(x, t) \quad , \quad 0 < x < 1 \text{ and } 0 \leq t \leq \Delta t \quad (3.16)$$

subject to the initial condition

$$D_3(x, 0^+) = D_3^n(x) \quad , \quad 0 \leq x \leq 1. \quad (3.17)$$

The updated value of D_3 , namely $D_3^{n+1}(\cdot)$, is the solution to (3.16) and (3.17) at $t = \Delta t$. We complete the process by updating $R(\cdot)$. This is accomplished by solving

$$\mathcal{R}(x) \left| \frac{\partial p}{\partial x} \right| (x) = \hat{\tau}_y \left(D_3^{n+1}(x) \mathcal{R}(x) \left| \frac{\partial p}{\partial x} \right| (x) \right) \quad (3.18)$$

and then defining $R^{n+1}(\cdot)$ by

$$R^{n+1}(x) = \min(1, \mathcal{R}(x)) \quad , \quad 0 \leq x \leq 1. \quad (3.19)$$

When solving (3.14) and (3.16) we let N be an integer, $\Delta x = \frac{2}{2N+1}$, and evaluate p and (D_3, R) on the respective grids

$$\left\{ x_k^1 = \frac{(2k-1)}{2} \Delta x \quad , \quad 1 \leq k \leq N+1 \right\} \quad (3.20)$$

and

$$\{ x_k^2 = (k-1) \Delta x \quad , \quad 1 \leq k \leq N \} . \quad (3.21)$$

All of our simulations were run with the following system parameters

$$s_2 = 1 \quad , \quad s_1 = .75 \quad , \quad D_1 = 2 \quad , \quad \text{and } q_0 = .135. \quad (3.22)$$

This choice of q_0 was well within the interval where the steady response curve $q_0 \rightarrow g(q_0)$ was decreasing. All simulations were carried out with $N = 100$ and $\Delta t = \min(\frac{1}{10N^2}, .035714 \epsilon_3)$ and explicit algorithms were used to update p and D_3 .

This first simulation was run with $\epsilon_3 = 7 \times 10^{-5}$ and the initial data $\hat{p}(x) = .995(1 - x)$, $0 \leq x \leq 1$. The solution with this data rapidly converges to an oscillatory right propagating wave train exhibiting regular relaxation oscillations. The speed of individual pulses is 0(100), a number far greater than the dimensionless average flow velocity which varies between .25 and .36.

Figure 5 shows relevant flow information at $t = .2$. The first frame in this figure shows the steady flow response curve and a graph of the negative pressure gradient versus the cross-sectional flow rate; i.e. the curve $x \rightarrow (q(x, .2), -\frac{\partial p}{\partial x}(x, .2))$. The point labeled + is the image of $x = 0$ and the point labeled o is the image of $x = 1$. The second frame shows profiles of p , $-\frac{\partial p}{\partial x}$, q , and R at $t = .2$. The remaining three frames are temporal plots of the exit flow rate, exit radius, and $10000 \times$ inlet pressure over the window [.18, .2].

The second simulation was run with $\epsilon_3 = 3.5 \times 10^{-5}$ and the same initial data as the first simulation. By time $t = .2$ the solution had converged to a regular relaxation oscillation whose temporal frequency is approximately twice that of the preceding simulation. This is easily seen by counting the number of spikes in the exit flow quantities over the window of length .02. Figure 6 shows the results of this simulation. A film of both simulations may be found at <http://www.math.cmu.edu/math/people/greenberg.html>.

Concluding Remarks

We note that once the extrudate exits the rheometer it is quenched leaving a solid tube as the final manufactured product. The wrinkles observed in the final product result from the oscillations in the exit radius, R , since the less viscous fluid is partially removed during the quenching and solidification process.

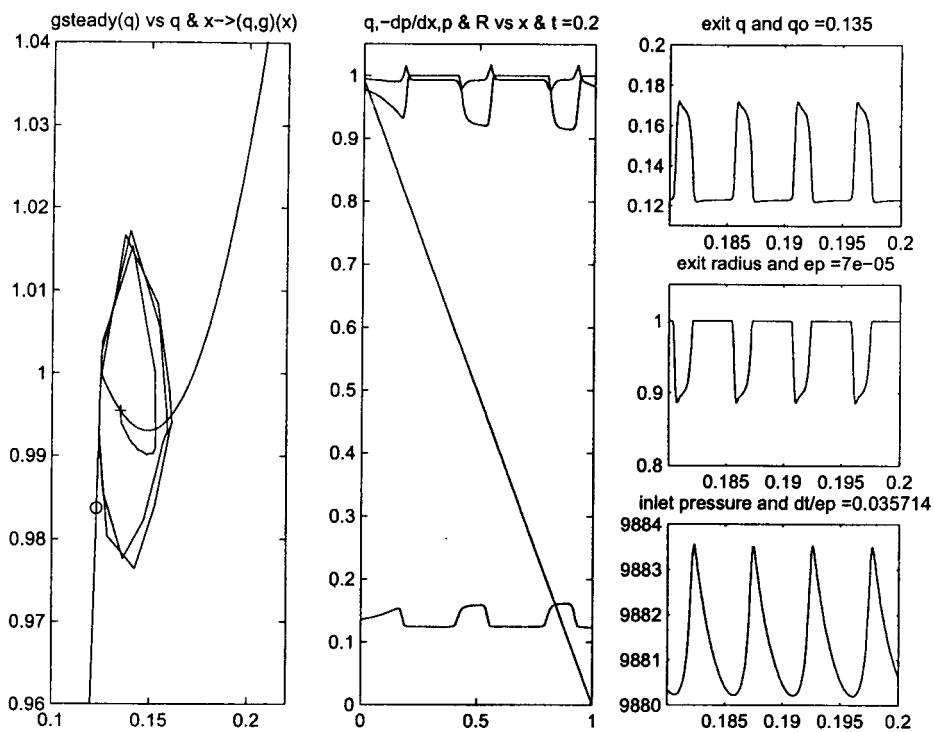


Figure 5

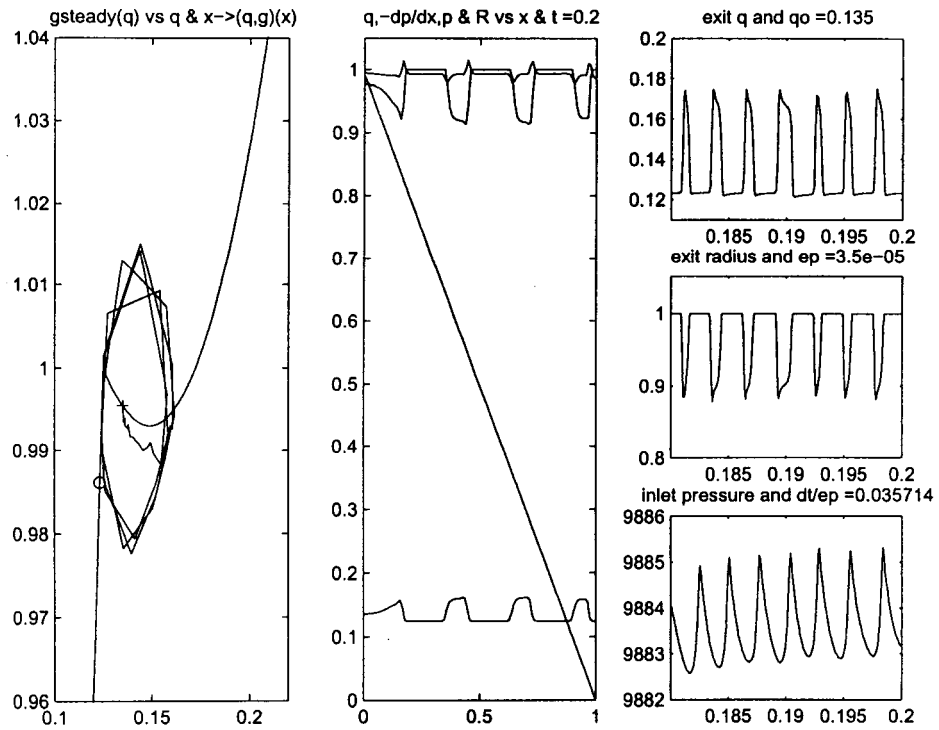


Figure 6

References

- [1] Greenberg, J.M. and Y. Demay, "A simple model of the melt fracture instability," *Euro. Jnl of Applied Mathematics* (1994), **5** 337-357.
- [2] Hatzikiriakos, H.A. & Dealy, J.M., "Wall slip on molten high density polyethylenes. II. Capillary rheometer studies," *J. Rheol.* (1992) **4** (36), 703-741.
- [3] Hatzikiriakos, H.A. & Dealy, J.M., "Role of slip and fracture in the oscillating flow of HDPE in a capillary," *J. Rheol.*, (1992) **5** (36), 845-884.
- [4] Joseph, D.D., Renardy, Y., *Fundamental of Two-Fluid Dynamics, Part I: Mathematical Theory and Applications*, Springer-Verlag, Vol. 3, 1993, pp. 375-378.